

Comparative analysis of tunneling magnetoresistance in low- T_c Nb/AlAlOx/Nb and high- T_c Bi_{2-y}Pb_ySr₂CaCu₂O_{8+δ} intrinsic Josephson junctions

V. M. Krasnov,* H. Motzkau, T. Golod, A. Rydh, and S.O. Katterwe
Department of Physics, Stockholm University, AlbaNova University Center, SE-10691 Stockholm, Sweden

A.B. Kulakov

Institute of Solid State Physics, Russian Academy of Sciences, 142432 Chernogolovka, Russia

(Dated: July 19, 2018)

We perform a detailed comparison of magnetotunneling in conventional low- T_c Nb/AlAlOx/Nb junctions with that in slightly overdoped Bi_{2-y}Pb_ySr₂CaCu₂O_{8+δ} [Bi(Pb)-2212] intrinsic Josephson junctions and with microscopic calculations. It is found that both types of junctions behave in a qualitatively similar way. Both magnetic field and temperature suppress superconductivity in the state-conserving manner. This leads to the characteristic sign-change of tunneling magnetoresistance from the negative at the sub-gap to the positive at the sum-gap bias. We derived theoretically and verified experimentally scaling laws of magnetotunneling characteristics and employ them for accurate extraction of the upper critical field H_{c2} . For Nb an extended region of surface superconductivity at $H_{c2} < H < H_{c3}$ is observed. The parameters of Bi(Pb)-2212 were obtained from self-consistent analysis of magnetotunneling data at different levels of bias, dissipation powers and for different mesa sizes, which precludes the influence of self-heating. It is found that $H_{c2}(0)$ for Bi(Pb)-2212 is $\simeq 70$ T and decreases significantly at $T \rightarrow T_c$. The amplitude of sub-gap magnetoresistance is suppressed exponentially at $T > T_c/2$, but remains negative, although very small, above T_c . This may indicate existence of an extended fluctuation region, which, however, does not destroy the general second-order type of the phase transition at T_c .

PACS numbers: 74.55.+v 74.25.Op 74.72.Gh 74.50.+r

I. INTRODUCTION

Magnetoresistance (MR) is one of the basic tools for analysis of the electronic structure of metals. MR data contains important information about *bulk* electronic structure of cuprate high temperature superconductors. This was demonstrated by recent MR studies providing compelling evidence for reconstruction of the Fermi surface in the pseudogap state of underdoped cuprates as a result of density wave ordering [1, 2]. Several experimental techniques revealed the existence of two distinct energy scales in cuprates: the superconducting gap Δ and the normal state pseudogap (PG) (for review, see e.g. Refs.[3–6]) with different behavior with respect to temperature [3, 7–13], doping [1, 14, 15] and magnetic field [16–18]. However, there is no consensus on whether they are competing [13, 19], cooperating [5], or representing two manifestations of the same phenomenon [5, 6, 20, 21].

Analysis of magnetic field effects is particularly useful for scrutinizing the superconducting origin of the gaps. Non-superconducting (e.g., structural, antiferromagnetic, charge, spin, or d -density wave) orders are typically insensitive to achievable fields [19]. In this case, magnetic field may selectively suppress the superconducting gap. However, discussion of magnetic field effects in cuprates remains controversial. Conflicting reports exist even on such a basic parameter as the upper critical

field H_{c2} . It was reported that H_{c2} behaves in a conventional manner, i.e., vanishes at T_c and scales with T_c as a function of doping [22–26]. But it was also reported that H_{c2} is T -independent and persists well above T_c [21] and increases with underdoping despite reduction of T_c [27].

There are many obstacles for deciphering MR data of cuprates such as: fuzzy superconducting transition due to persistence of the PG; d -wave symmetry of Δ ; ill defined quasiparticles (QP) and strong angular dependence of QP scattering rates [28]; very high anisotropy, which requires accurate control of transport current direction and sample geometry; existence of an extended fluctuation region above T_c [29]; possible doping inhomogeneity [6]; and extremely large $H_{c2} \sim 100$ T. One of the important open question is whether so large magnetic fields simply suppress superconductivity, or simultaneously induce a competing order, as may be suggested by observation of charge density [6] and antiferromagnetic spin order [30] in vortex cores.

Typically MR involves only QPs at the Fermi level, averaged over the Brillouin zone, and thus does not provide spectroscopic information about the QP density of states (DOS) away from the Fermi surface. A rare exception is the c -axis transport in extremely anisotropic layered cuprates. Single crystals of Bi, Tl [31, 32] and Hg [33] based cuprates represent natural stacks of atomic scale intrinsic tunnel junctions. The intrinsic tunnelling spectroscopy (ITS) provides a unique opportunity to probe directly bulk electronic spectra of cuprates [7, 10, 13, 18, 34]. Tunneling MR is potentially a very powerful tool for analysis of superconducting features in

* Vladimir.Krasnov@fysik.su.se

electronic spectra. This was demonstrated in previous studies for cuprates [16, 18, 35–37] as well as for conventional low- T_c [38–40] and non-cuprate [41] high T_c superconductors. Application of magnetic field leads to appearance of a spatially inhomogeneous mixed state. This makes analysis of magnetotunneling data non-trivial [42, 43] and even counterintuitive [44]. Therefore, a clear understanding of how the magnetotunneling characteristics of Josephson junctions should behave is needed for accurate data analysis.

In this work we perform detailed comparison of magnetotunneling in low- T_c Nb/AlAlOx/Nb, and slightly overdoped $\text{Bi}_{2-y}\text{Pb}_y\text{Sr}_2\text{CaCu}_2\text{O}_{8+\delta}$ [Bi(Pb)-2212] intrinsic Josephson junctions with theoretical calculations. Small sizes of our Bi(Pb)-2212 mesas, which are one-two orders of magnitude smaller than in previous similar studies [16, 18, 36], in combination with the ability to extract information at the sub-gap bias with low dissipation power, lead to effective obviation of self-heating [13, 45, 46]. Both low- and high- T_c junctions show qualitatively similar behavior. Magnetic field and temperature suppress superconductivity in the state-conserving manner: enhancement of the sub-gap conductance due to suppression of $\Delta(T, H)$ is exactly compensated by reduction of the sum-gap conductance peak. As a result, the MR changes sign from the negative at the sub-gap voltages to the positive at the sum-gap $eV \gtrsim 2\Delta$. This allows us to trace closing of Δ at $T \rightarrow T_c$ with unprecedented clarity. We derive simple scaling laws for magnetotunneling and employ them for unambiguous extraction of superconducting parameters such as $\Delta(T, H)$ and $H_{c2}(T)$. The extracted $H_{c2}(T)$ decreases significantly upon approaching T_c . Our data indicates that superconductivity in slightly overdoped cuprates appears in a conventional manner by means of the second order phase transition.

The paper is organized as follows. In sec. II we describe the theoretical formalism, used for microscopic calculation of current-voltage ($I - V$) characteristics in the mixed state. Sec. III describes the experimental setup and studied junctions. Methods used for obviation of self-heating are discussed. In sec. IV we present main results. It is shown that both Nb and Bi-2212 junctions behave in a qualitatively similar way as a function of T and H . In sec. V we analyze scaling laws of different tunneling parameters as a function of H/H_{c2} and apply them for extraction of H_{c2} in Nb-junctions. This also provides a clear evidence for persistence of the surface superconductivity in Nb. In sec. VI we apply the same scaling laws for extraction of $H_{c2}(T)$ for Bi(Pb)-2212 and analyze the remaining MR above T_c . Finally, in sec. VII we summarize our conclusions.

II. THEORY

To calculate spatially non-uniform distribution of the gap and the DOS in the mixed state, we use the circular cell approximation [47–49]. We approximate the hexago-

nal unit cell of the Abrikosov vortex lattice by a circular cell with a radius corresponding to one flux quantum Φ_0 within the cell, see the sketch in Fig. 1 (a),

$$\rho = \sqrt{\frac{\Phi_0}{\pi H}} \quad (1)$$

and assume a cylindrically symmetric vector potential

$$Q(r) = 1/r - r/\rho^2. \quad (2)$$

Spatial distribution of the order parameter $\Delta(r)$ at different temperatures and magnetic fields are calculated by solving microscopic Usadel equations:

$$\pi T_c \xi_S^2 \left[\Theta_n'' + \frac{\Theta_n'}{r} \right] - \omega_n \sin(\Theta_n) - \quad (3)$$

$$Q^2(r) \sin(\Theta_n) \cos(\Theta_n) + \Delta \cos(\Theta_n) = 0,$$

together with the self-consistency equation,

$$\Delta \ln(T/T_c) + 2\pi T \sum_n (\Delta/\omega_n - \sin(\Theta_n)) = 0. \quad (4)$$

Here $\xi_S = (D/2\pi T_c)^{1/2}$, where D is the QP diffusion coefficient, $\omega_n = \pi T(2n + 1)$, $n = 0, 1, 2, \dots$ are Matsubara frequencies, $\cos(\Theta_n)$ and $\sin(\Theta_n)$ are the normal and the anomalous Green function components, and primes denote spatial derivation $\partial/\partial r$. Those equations are subject to boundary conditions at the center of the vortex $r = 0$: $\Delta(0) = \Theta_n(0) = 0$, and at the edge of the circular cell $r = \rho$: $\Delta(\rho)' = \Theta_n(\rho)' = 0$. This system of nonlinear equations was solved numerically, up to a cut-off frequency $n \simeq 50 T_c/T$, using an iterative procedure. More details about the formalism and the numerical procedure can be found in Refs. [48–50].

Fig. 1 (b) shows an example of calculated spatial distribution of $\Delta(r)$ along the line connecting two vortices for the case of Nb ($T_c = 8.8K$) at $T = 4.7K$ and $H/H_{c2} = 0.5$. The $\Delta(r)$ is normalized by the equilibrium value of the gap $\Delta_0(T)$ at $H = 0$.

To calculate $I - V$ characteristics in the mixed state, we also need to calculate the spatial variation of the QP DOS $N(r, E)$ as a function of the QP energy E . This is done by analytic continuation of discrete $\Theta_n(\omega_n)$ to the continuous energy axis via substitution, $\omega_n = -iE$, in Eq. (3), where i is the imaginary unit:

$$\pi T_c \xi_S^2 \left[\Theta'' + \frac{\Theta'}{r} \right] + iE \sin(\Theta) - \quad (5)$$

$$Q^2(r) \sin(\Theta) \cos(\Theta) + \Delta(r) \cos(\Theta) = 0.$$

The spatially non-uniform DOS is then obtained as

$$N(r, E) = \Re(\cos[\Theta(r, E)]). \quad (6)$$

Lines in Fig. 1 (c) show $N(r, E)$, normalized to the DOS in the normal state, at three points of the circular cell: A - at the center of the vortex, B - at the intermediate point where $\Delta(r)$ recovers to half of its maximum value, see Fig. 1 (b), and C - at the edge of the

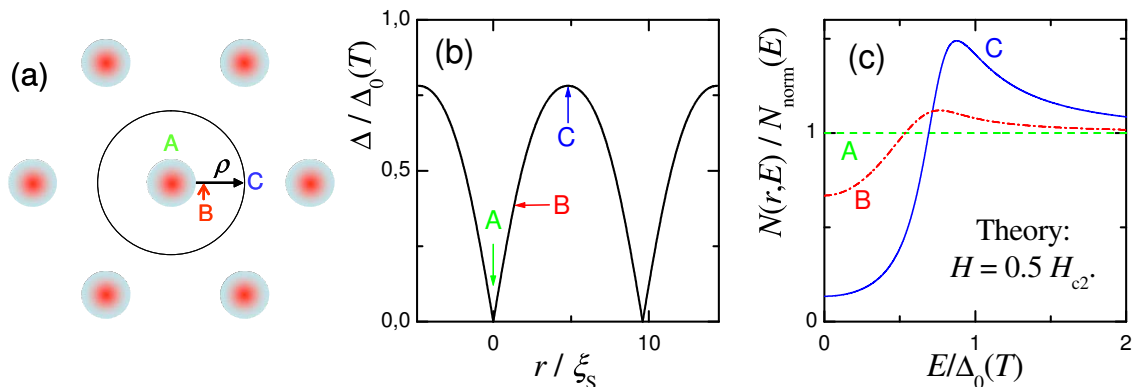


FIG. 1. (Color online). (a) A sketch of the hexagonal Abrikosov vortex lattice and the circular approximation of a unit cell. (b) Calculated spatial distribution of the order parameter between two vortices. (c) Local density of states at three points A, B, C, indicated in (a) and (b). Calculations are made for $H = 0.5 H_{c2}$, $T = 4.7$ K and $T_c = 8.8$ K.

cell. In the center of the vortex the superconductivity is completely suppressed, $\Delta = 0$, and $N(E) = 1$, as in the normal state. Away from the vortex the order parameter is partly restored, but QP spectra are gapless $N(E < \Delta) \neq 0$ [38–40]. Due to spatial inhomogeneity, the maximum in DOS is significantly smeared, compared to the BCS singularity, and the energy of the maximum is no longer equal to $\Delta(r)$.

Tunneling $I - V$ characteristics are calculated by integration over the circular unit cell:

$$I(V) = \frac{1}{R_n} \int_0^\rho \frac{2r}{\rho^2} dr \int_{-\infty}^{+\infty} dE \quad (7)$$

$$N(r, E)N(r, E + eV)f(E)[1 - f(E + eV)].$$

Here R_n is the tunneling (normal) resistance and f is the Fermi distribution function.

A. Validity of the model

The described formalism is valid for arbitrary T and H for dirty type-II superconductors with s -wave symmetry of the order parameter, which is appropriate for sputtered Nb films. Calculations presented below are made for BCS parameters with $T_c = 8.8$ K, typical for Nb. This allows direct comparison with experimental data for Nb/AlAlOx/Nb junctions.

In Eq. (7) we disregard possible misalignment of vortices in the two electrodes. For intrinsic Josephson junctions, due to very high anisotropy and weak interlayer coupling, such misalignment may be significant at low magnetic fields [42], but could be neglected for high fields used in this work.

Certain deviations can be expected for Bi-2212 due to the d -wave symmetry of the order parameter, which reduces the sum-gap singularity and affects the vortex structure [51–53]. However, theoretical calculations

demonstrated [42, 51] that the scaling of DOS characteristics as a function of H/H_{c2} , which will be discussed below, is valid also for d -wave superconductors (see e.g. Figs. 5 from Ref. [51]). Therefore, the procedure of extraction of H_{c2} from such a scaling should be also valid for intrinsic Josephson junctions.

Coexistence of competing order parameters, associated with the pseudogap, could also affect the tunneling DOS in cuprates [54, 55]. An influence of the PG on the intrinsic tunneling MR was reported for underdoped Bi-2212 [16, 18, 27, 36, 43]. Namely, with underdoping the sub-gap MR is rapidly reduced [27] and suppression of superconductivity by magnetic field occurs in a seemingly non-state-conserving manner [36]. This may indicate a gradual recovery of the competing PG order upon suppression of superconductivity, as observed in the vortex cores [6, 30]. To avoid possible complications, we restrict our analysis to slightly overdoped Bi(Pb)-2212, for which there is no significant distortion by the PG [13, 56].

III. EXPERIMENTAL

We study tunneling magnetoresistance in standard low- T_c Nb/AlAlOx/Nb junctions and in small slightly overdoped Bi(Pb)-2212 mesa structures containing few atomic scale intrinsic Josephson junctions. Measurements were performed in a gas-flow ^4He cryostat in a temperature range down to 1.6 K and magnetic field H up to 17 T. Samples were mounted on a rotatable sample holder with the alignment accuracy better than 0.02° . Details of the measurement setup can be found in Refs. [34, 57].

A. Nb/AlAlOx/Nb junctions

Nb/AlAlOx/Nb junctions were made by the standard HYPRES trilayer technology [58] with a critical current

density of 1000 A/cm^2 . A detailed description of junction parameters can be found in Ref. [59]. Junctions consist of two sputtered Nb thin films with thicknesses 150 and 50 nm for base and counter electrodes, respectively. Due to different thicknesses, electrodes have slightly different T_c . The critical temperature of the junction is $\simeq 8.8 \text{ K}$. The junction barrier is formed by deposition of a thin Al layer with the thickness $\sim 10 \text{ nm}$ on top of the base electrode, followed by a subsequent oxidation to form the AlOx tunnel barrier. During oxidation, only the surface layer of Al is oxidized, leaving the rest of Al intact. This results in a proximity effect between the bottom Nb layer and Al [50]. Tunneling occurs between the proximity-induced superconducting layer of Al and the top Nb layer. A detailed analysis of the proximity effect in Nb/ AlAlOx /Nb junctions can be found in Ref. [50].

Several junctions with different sizes on the same chip were studied and showed similar results. As for the case of Bi-2212 mesas [13], with increasing junction area the sum-gap kink in $I-V$ becomes excessively sharp and may even develop a back-bending as a result of progressive self-heating [60]. Self-heating is effectively obviated by miniaturization of junctions [13, 45, 46]. Therefore, in what follows we show data only for the smallest junction with sizes $\sim 2.5 \times 2.5 \mu\text{m}^2$, which is least affected by self-heating.

B. Bi-2212 intrinsic Josephson junctions

We study small, micrometer-size mesa structures containing few atomic scale intrinsic Josephson junctions. The mesas are fabricated on top of Bi-2212 single crystals using micro/nano-fabrication techniques. Details of the crystal growth and sample fabrication can be found in Refs. [61] and [62], respectively. Several contacts on top of the crystals allow us to perform three or quasi-four probe measurement of the pure c -axis transport [63]. Details of measurements and mesa characterization can be found elsewhere [13, 14, 34].

We present data for two batches of crystals: lead-doped, slightly overdoped $\text{Bi}_{2-y}\text{Pb}_y\text{Sr}_2\text{CaCu}_2\text{O}_{8+x}$ with $T_c \simeq 89 - 93 \text{ K}$ and yttrium-doped, slightly underdoped $\text{Bi}_2\text{Sr}_2\text{Ca}_{1-x}\text{Y}_x\text{Cu}_2\text{O}_{8+x}$ (Bi(Y)-2212) with $T_c \simeq 92 \text{ K}$. It should be said that the c -axis phase coherence in small mesas is not a good measure of T_c . The associated Josephson coupling energy density is small, and the total energy is decreasing proportional to the mesa area. Therefore, in small mesas the phase coherence and the c -axis critical current are suppressed by thermal fluctuations [62, 64] at temperatures significantly lower than that for the in-plane transport. A more detailed discussion on determination of T_c can be found in Ref. [13]. Both types of crystals have similar optimal $T_c \simeq 96 \text{ K}$. The most noticeable difference between them is in the c -axis critical current density $J_c(4.2 \text{ K}) \simeq 10^4$ and 10^3 A/cm^2 for lead- and yttrium-doped mesas, respectively. This is due to a rapid increase of J_c with

over-doping [14].

The c -axis transport in Bi-2212 is non-metallic due to interlayer tunneling mechanism of transport, in combination with the so-called c -axis pseudogap. The latter is much more pronounced than the PG in the ab -plane transport [4, 9, 65] and exists in a broader temperature [7, 14] and doping ranges [6]. In Ref. [34] it was shown that in the normal state $T > T_c$, c -axis intrinsic tunneling characteristics exhibit a trivial thermal-activation behavior, described by just one constant - the effective barrier height. This puts a question whether the c -axis PG represents the real two-particle gap in the DOS or is just the single QP tunneling matrix phenomenon. In Ref. [13] more subtle features in intrinsic tunneling characteristics were found beyond the thermal-activation background. Those appear in the same temperature region as in the ab -plane transport and were attributed to the genuine two-particle pseudogap in the QP DOS. A similar conclusion about the existence of two distinct pseudogap-like phenomena above T_c was also reached in optical infrared ellipsometry studies [9, 65]. The PG complicates analysis of tunneling magnetoresistance because it makes the superconducting transition fuzzy. Since the main purpose of this work is to establish how to extract unambiguous information out of magnetotunneling data, here we will mostly concentrate on analysis of overdoped Bi(Pb)-2212 crystals, which according to previous studies are less affected by the PG and are most close to the conventional BCS-type superconductivity [56].

C. Obviation of self-heating in Bi-2212 mesas

Mesas with different sizes were made on the same single crystal. As in the case of Nb/ AlAlOx /Nb junctions [60], we observe that $I-V$ characteristics of larger mesas are more distorted by self-heating at large bias [13]. To obviate self-heating, we perform additional miniaturization of mesa structures [13, 45, 46] down to sub-micrometer sizes using Focused Ion Beam trimming [62].

The dissipation powers at the sum-gap knee in $I-V$ (the peak in dI/dV) for the two small mesas shown in Fig. 2 (c) and (d) are $P \simeq 0.13$ and 0.19 mW for Bi(Pb)-2212 and Bi(Y)-2212 mesas, respectively, at the lowest temperatures. According to previous reports [13, 46], typical thermal resistances of our micrometer-size mesas lie in the range $\sim 70 - 30 \text{ K/mW}$ at low T and decrease to $\sim 10 \text{ K/mW}$ at T_c . Thus, self-heating at the sum-gap peak for those small mesas is manageable and the effective mesa temperature at the peak remains well below T_c . For the Bi(Y)-2212 mesa this was unambiguously proven by analysis of the size-dependence of intrinsic tunneling spectra for mesas with different sizes on the same single crystal [13, 46]. To completely exclude possible artifacts of self-heating from the data analysis, in what follows we define superconducting parameters from scaling laws valid for tunneling magnetoresistance at different bias levels, including low, sub-gap bias with negligible heating.

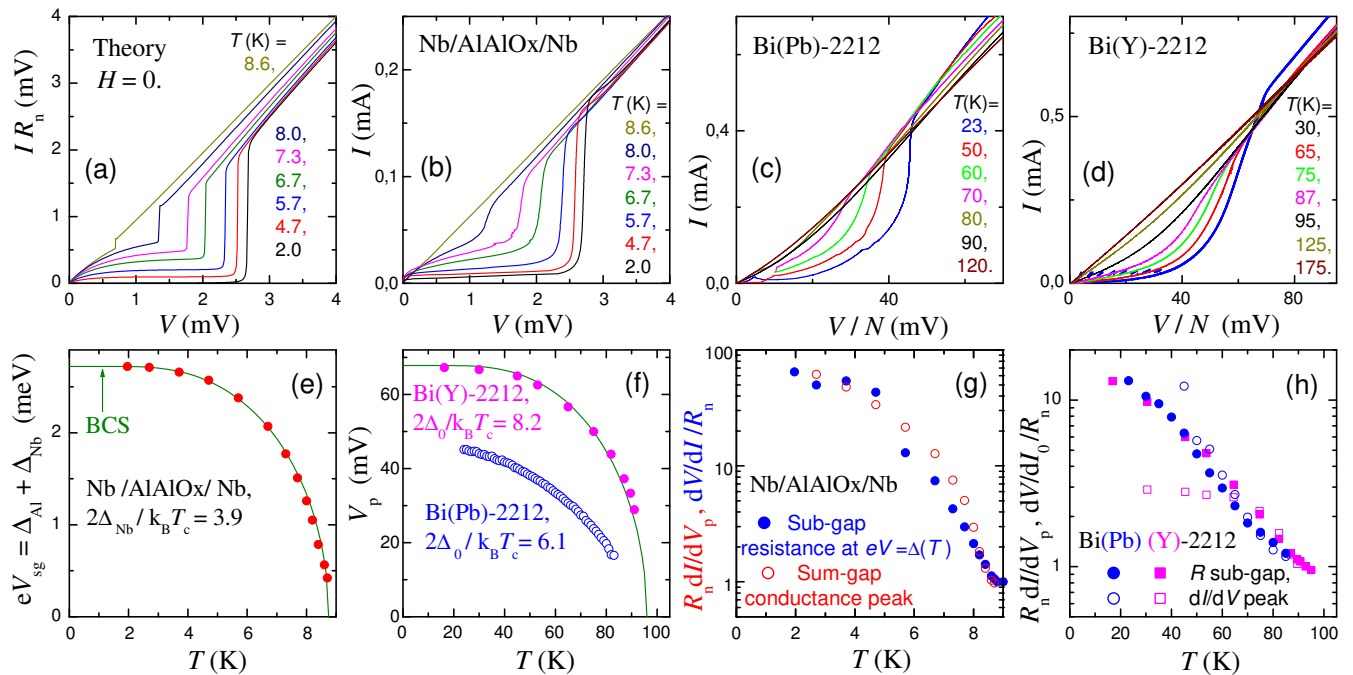


FIG. 2. (Color online). Temperature dependence of tunneling $I - V$ characteristics at zero magnetic field for (a) calculations for a BCS superconductor (Nb, $T_c = 8.8$ K), (b) for the Nb/AlAlOx/Nb junction, (c) for slightly overdoped Bi(Pb)-2212 mesa and (d) for slightly underdoped Bi(Y)-2212 mesa. (e) and (f) Measured T -dependence of the sum-gap voltage. Solid lines represent BCS T -dependence. (g) and (h) Comparison of the correlation between the sub-gap resistance (solid symbols) and the sum-gap conductance (open symbols) for the same Nb/AlAlOx/Nb junction and Bi-2212 mesas, respectively.

IV. RESULTS AND DISCUSSION

A. Temperature dependence of tunneling characteristics at zero magnetic field

Figure 2 shows T -dependencies of $I - V$ s at $H = 0$ for (a) theoretical calculations for Nb parameters, (b) the Nb/AlAlOx/Nb junction, (c) a slightly overdoped Bi(Pb)-2212 mesa with the in-plane area $0.9 \times 1.3 \mu\text{m}^2$ and $T_c \simeq 91$ K and (d) a slightly underdoped Bi(Y)-2212 mesa with the area $1.8 \times 2.0 \mu\text{m}^2$ and $T_c \simeq 92$ K. Both mesas contain $N = 9$ intrinsic Josephson junctions, estimated by counting QP-branches in $I - V$ [13]. It is seen that $I - V$ s of Bi-2212 mesas are closely resembling those for conventional superconductor-insulator-superconductor tunnel junctions. The pronounced sum-gap kink is clearly seen at low temperatures, followed by an almost T -independent tunneling resistance at higher bias. The sum-gap kink moves to lower voltage and vanishes in amplitude upon approaching the T_c [7, 13].

Experimental characteristics of the Nb/AlAlOx/Nb junction can be explicitly compared with the corresponding theoretical simulations. It is seen that there is a good agreement, however, the proximity effect between Al and Nb leads to some smearing out of the sum-gap kink and enhancement of the sub-gap conductivity. The most clear proximity induced peculiarity in $I - V$ of Nb/AlAlOx/Nb is the pronounced dip in dI/dV above the sum-gap peak

(see Fig. 4 b). The dip is caused by the double maxima structure of the DOS in Al [50]: the lower maximum corresponds to the proximity induced energy gap in Al, Δ_{Al} , the upper - to the inherited gap from Nb, Δ_{Nb} . In this case the sum-gap peak in conductance occurs at $eV_{sg} = \Delta_{Al} + \Delta_{Nb}$ and the dip at $eV \simeq 2\Delta_{Nb}$. Thus determined gaps are: $\Delta_{Al} = 1.22$ meV and $\Delta_{Nb} = 1.49$ meV, consistent with previous reports [50].

Due to the d -wave symmetry of the order parameter in cuprates, the sum-gap kinks in Bi-2212 intrinsic tunneling characteristics are significantly more smeared than in s -wave low- T_c junctions. From comparison of Figs. 2 (c) and (d) it is also clear that the sum-gap kink is further losing its sharpness with underdoping [14].

Figure 2 (e) and (f) represent T -dependencies of the sum-gap voltage (peak in dI/dV) at $H = 0$ for the Nb/AlAlOx/Nb junction and the Bi-2212 mesas (per intrinsic Josephson junction), respectively. They were obtained from $I - V$ shown in Figs. 2 (b-d). The bulk gap of Bi(Y)-2212 follows very accurately the standard BCS dependence. More details on the T -dependence of inter-layer tunneling characteristics of our mesas can be found in Refs. [13, 34].

Both Nb and Bi-2212 demonstrate signatures of strong coupling superconductivity. For Nb the ratio $2\Delta_{Nb}/T_c \simeq 3.9$, larger than the weak coupling BCS value of 3.5 for s -wave superconductors. For the slightly underdoped Bi(Y)-2212, $2\Delta_0/T_c \simeq 8.2$. In the slightly overdoped

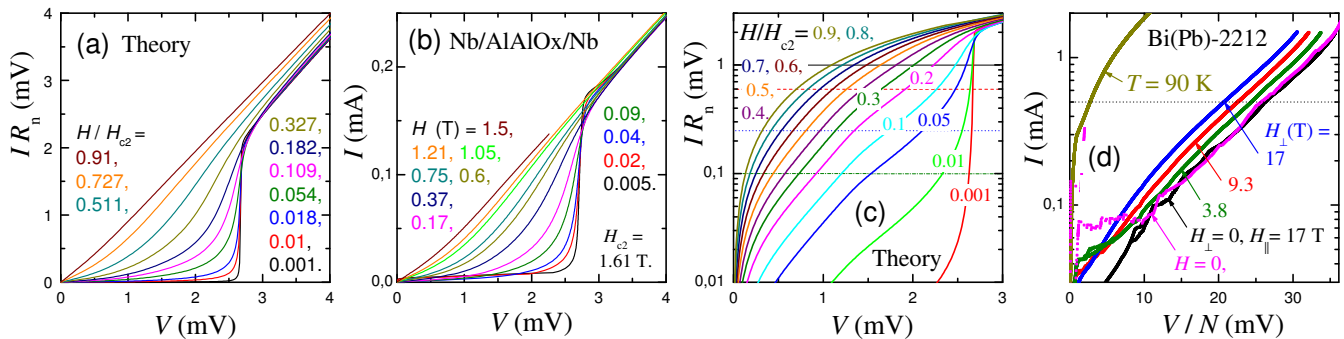


FIG. 3. (Color online). Magnetic field evolution of $I - V$ characteristics at low T for (a) BCS calculations at $T \simeq 2$ K and $T_c = 8.8$ K, (b) the Nb/AlAlOx/Nb junction at $T \simeq 2$ K. Semi-logarithmic plots of (c) theoretical $I - V$ s at $T \simeq 0.5$ K, and (d) $I - V$ s of a Bi(Pb)-2212 mesa in the sub-gap region at $T \simeq 2$ K for different c -axis field components. Note a remarkable almost parallel translation of $I - V$ s in the semi-logarithmic scale in (c) and (d).

Bi(Pb)-2212, the ratio decreases to 6.1. This is consistent with previous break junction studies, which indicated that in overdoped Bi-2212 $2\Delta_0/T_c$ is approaching the weak coupling BCS value for d -wave superconductors of 4.28 [56].

As seen from Figs. 2 (b-d) in all cases the increase of T leads to simultaneous increase of the sub-gap current and decrease of the sharpness of the sum-gap kink. To demonstrate this reciprocal correlation, in Figs. 2 (g) and (h) we plot the T -dependence of the sub-gap resistance, $dV/dI(V = \Delta/e)$, (solid symbols) and the sum-gap conductance peak, $dI/dV(V = 2\Delta/e)$, (open symbols) for the same junctions. For Nb/AlAlOx/Nb the correlation is observed in the whole temperature range. For Bi-2212 the correlation is holding well until $\sim T_c/2$. The deviations at lower temperatures are caused by two artifacts affecting the sum-gap peak height. For Bi(Pb)-2212 the peaks becomes sharper because of self-heating and for Bi(Y)-2212 it becomes broader because of minor inhomogeneity of junctions in the mesa [13, 66].

B. Analysis of tunneling magnetoresistance

Figs. 3 (a) and (b) show calculated and measured $I - V$ s of Nb/AlAlOx/Nb at $T \simeq 2$ K for different out-of-plane magnetic fields. Again, a good agreement is seen. With increasing field, the sub-gap current increases and the sum-gap kink is rapidly smeared out. The $I - V$ is approaching the ohmic normal-state at $H \rightarrow H_{c2}$.

From comparison of theoretical curves in Figs. 2 (a) and 3 (a) it is seen that although both temperature and magnetic field suppress superconductivity when $T \rightarrow T_c$ and $H \rightarrow H_{c2}$, there is a difference in how they do that. Namely, the temperature reduces Δ but does not affect the shape of the QP DOS, which remains gapped $N(E < \Delta) = 0$ and maintains a sharp BCS singularity at the gap. Because of that the sum-gap kink remains sharp even at elevated T . On the other hand, magnetic field first of all smears the gap singularity in the DOS and the sum-gap

kink in $I - V$ and increases the sub-gap conductance by making the DOS gapless.

Figure 3 (c) shows simulated $I - V$ at different H and at $T = 0.5$ K in the semi-logarithmic scale. It is seen that in this scale the curves remain almost parallel and move to lower voltage with increasing H (negative MR).

Fig. 3 (d) represents the similar semi-logarithmic plot of $I - V$ curves at different H and at $T = 2$ K for a larger Bi(Pb)-2212 mesa on the same crystal as in Fig. 2 (c). Here we changed the c -axis component of the field H_\perp from 0 to 17 T by rotating the crystal with respect to the fixed magnetic field of 17 T. Because of the extreme anisotropy of Bi-2212, in-plane magnetic field of 17 T does not produce any effect on QP DOS. This is clearly seen from the two rightmost $I - V$, which were measured at $H = 0$ (magenta) and at $H = 17$ T strictly parallel to the ab -planes (black). The only minor difference between those curves is caused by appearance of phonon-polariton resonances [67], seen as small steps in $I - V$.

Clearly, the general trend of experimental $I - V$ for Bi-2212 is the same as for numerical simulations and Nb/AlAlOx/Nb: in the semi-logarithmic scale the curves remain parallel and move to lower voltages, as the consequence of suppression of the superconducting gap by field. A similar trend was also observed for Bi-2212 intrinsic Josephson junctions as a function of T [13, 34]. For comparison, in Fig. 3 (d) we also show the $I - V$ at $T = 90$ K $\simeq T_c$ at $H = 0$. Apparently, the maximum available field of 17 T is insufficient for complete suppression of superconductivity at $T = 2$ K. The parallel shift of $I - V$ curves implies that the MR, $V(I, H = 0) - V(I, H)$, measured at fixed current and T , is approximately bias-independent. This is important because it allows a confident estimation of the MR in a broad sub-gap bias range, including low bias with low dissipation powers, which precludes distortion by self-heating.

Fig. 4 shows tunneling conductance $dI/dV(V)$ curves in the semi-logarithmic scale at low $T \simeq 2$ K and at different out-of-plane magnetic fields. Panels (a) and (b) correspond to theoretical and experimental data for the

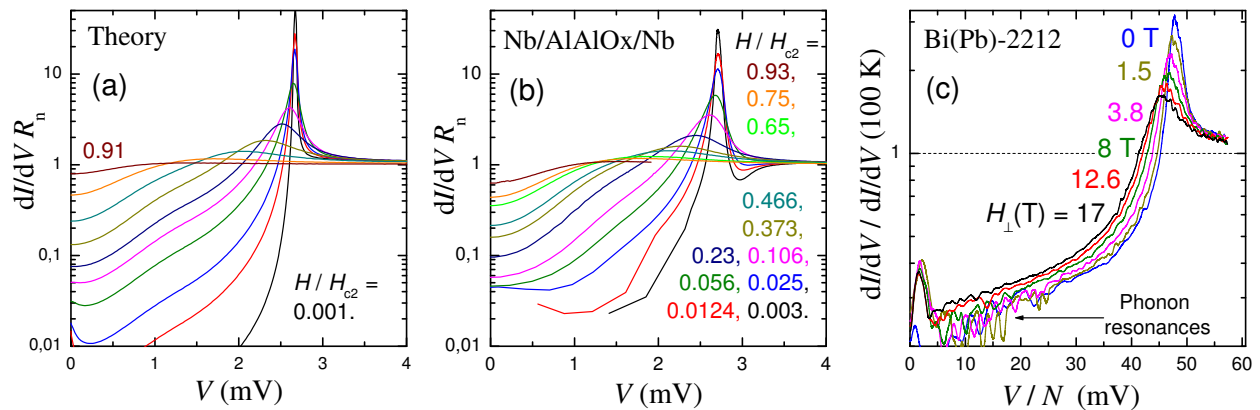


FIG. 4. (Color online). Magnetic field evolution of $dI/dV(V)$ characteristics at low T : (a) BCS calculations at $T = 2$ K, (b) the Nb/AlAlOx/Nb junction at $T = 2$ K and (c) a small Bi(Pb)-2212 mesa (normalized by $dI/dV(T \gtrsim T_c)$) at $T = 1.7$ K. All plots are shown in the semi-logarithmic scale. Low bias structure in (c) is caused by excitation of phonon-polariton resonances by the ac-Josephson effect [67]. Due to state conservation, the magnetoresistance is negative in the sub-gap region, but positive at and above the sum-gap peak. Note also an almost parallel translation of $\ln dI/dV(V)$ curves with H .

Nb junction from Figs. 3 (a) and (b), respectively. At zero field the main feature of $dI/dV(V)$ curves is the sharp sum-gap peak at $V_p = 2\Delta/e$, which reflects the sharp BCS singularity in the QP DOS at $E = \Delta$. With increasing field, the peak is rapidly smeared out. Already at $H = 0.1 H_{c2}$ the height of the peak is suppressed by an order of magnitude. Simultaneously the sub-gap conductance at $V < V_p$ is growing with field. The excess QP current is flowing in gapless vortex cores, see Fig. 1 (a). It scales with the relative core area in the unit cell and, therefore, increases approximately linearly towards the normal conductance at $H \rightarrow H_{c2}$.

In Fig. 4 (c) we show $dI/dV(V)$ characteristics in the semi-logarithmic scale for different H_{\perp} at $T = 1.7$ K, for another mesa $1 \times 1.9 \mu\text{m}^2$ on the same Bi(Pb)-2212 single crystal. To simplify the analysis, the curves are normalized by the normal state curve at $T = 100$ K, so that the normal state is simply represented by the dashed horizontal line. It is seen that $dI/dV(V)$ curves shift as a whole to lower voltages with increasing field. Simultaneously the peak loses the height while the sub-gap conductance vice-versa increases with increasing field. Such the behavior is almost identical to that for the Nb/AlAlOx/Nb junction and calculations, shown in Figs. 4 (a) and (b).

C. State conservation

According to theory, suppression of superconductivity both by temperature and magnetic field occurs in the state-conserving manner. Even though superconductor-insulator-superconductor tunneling is not probing explicitly the single QP DOS, but rather the convolution of two DOS from the two electrodes, Eq. (7), it is still possible to judge about the state conservation by a simple inte-

gration of dI/dV curves:

$$\int_0^{\infty} \left(R_n \frac{dI}{dV} - 1 \right) dV = 0. \quad (8)$$

The state conservation is the reason for T - and H -independence of the large bias tunneling resistance R_n , as seen from Figs. 2 (a) and 3 (a).

From Figs. 2 (b-d) it is clear that both in low- T_c and high- T_c junctions the Ohmic tunneling resistance R_n above the sum-gap kink is remaining almost T -independent. According to Eq. (8), this automatically implies that closing of the superconducting gap by temperature occurs in the state-conserving manner.

State conservation implies that the tunneling resistance is enhanced in the sub-gap region in the same manner as the conductance is enhanced at the sum-gap peak. This is demonstrated explicitly, in Figs. 2 (g) and (f) for Nb/AlAlOx/Nb and Bi-2212 junctions, respectively. It is seen that the sub-gap resistance dV/dI in the middle of the sub-gap region $eV = \Delta(T)$ and the sum-gap conductance peak grow in a similar manner with decreasing T . Such a scaling is an instructive way for examining the state conservation in Bi-2212 because it does not depend on a small $R_n(T)$ dependence [7, 34], which is likely due to a minor in-plane (coherent) contribution to the inter-layer transport [68].

D. The sign change of tunneling magnetoresistance

The tunneling MR in superconducting tunnel junctions and the c -axis MR in layered cuprates is often described as negative. That is, the resistance decreases with increasing field. This is the consequence of appearance of the gapless state in magnetic field. The corresponding increase of the sub-gap DOS leads to approximately linear increase of the low bias tunneling conductance with

field [43]. This is clearly seen in Fig. 4. However it is also seen that at the sum-gap peak the situation is reversed: the tunneling conductance is decreasing with increasing field, i.e., the tunneling MR at $V \gtrsim V_p$ is positive. Thus, the tunneling MR is changing sign from the negative at the sub-gap voltage to the positive close and above the sum-gap voltage. Again, the behavior is similar for both Nb/AlAlO_x/Nb and Bi(Pb)-2212 junctions.

The sign change of the tunneling MR is a direct consequence of state conservation. The missing area of the sub-gap conductance with respect to normal conductance $1/R_n$ is equal to the excess area of the sum-gap peak. Therefore, the positive MR at large bias is directly connected with the negative MR at low bias. The discussed sign-change of the MR is very characteristic and can be used for unambiguous discrimination of the superconducting gap from non-pairing effects in the tunneling DOS, such as peculiarities of one-QP band structure, or thermal activation enhancement of the tunneling matrix elements for interlayer hopping [34].

V. SCALING LAWS OF TUNNELING MAGNETORESISTANCE

The main purpose of this work is to determine how to extract useful information from tunneling MR. To understand this we first consider the behavior of magnetotunneling for conventional BCS superconductors. For this we analyze numerically calculated and experimental characteristics for Nb junctions at different T and H .

A. Zero-bias magnetoresistance

Transport measurements are usually performed by applying a small ac-current, i.e., probe zero-bias MR. Thick lines in Fig. 5 (a) show theoretical values of the zero bias conductance $dI/dV(0)$, normalized by R_n , as a function of H/H_{c2} for $T = 2, 4.7$ and 7.3 K. It is seen that at low $T = 2$ K, the zero bias conductance is gradually increasing from almost zero at $H = 0$, to normal conductance at $H_{c2}(T)$ (see Fig. 4 (a)).

Temperature dependence of $dI/dV(0)$ at $H = 0$ can be seen from $I - V$ curves in Fig. 2 (b). The increase of T leads to the decrease of Δ . Both factors result in the increased number of excited QPs above the gap, which initially leads to a rapid filling-in of the zero-bias dip in conductance and then to development of a maximum at $V = 0$. The latter represents a zero-bias logarithmic singularity [69]. It occurs because at elevated T there is a substantial amount of thermally excited QPs just above the gap. At $V = 0$ the partly filled gap singularities in the two electrodes are co-aligned, causing a large current flow from one electrode to another, which is exactly compensated by the counterflow from the second electrode. However, exact cancellation is lifted at an arbitrary small voltage across the junction, leading to a sharp maximum

in dI/dV . The zero-bias logarithmic singularity leads to an overshooting of $dI/dV(0)$ at $H = 0$ over the normal conductance at $T = 7.3$ K in Fig. 5 (a).

The zero-bias logarithmic singularity makes the behavior of the zero-bias conductance non-trivial. In general, there is no scaling with H/H_{c2} for $dI/dV(0)$ at different T , as seen from Fig. 5 (a). To avoid complications caused by the zero-bias singularity we look at the behavior of the conductance at finite bias.

B. Scaling of the sub-gap conductance and the sum-gap resistance

Fig. 5 (b) shows field dependence of the sub-gap conductance at the middle point $eV = \Delta$ for the same temperatures as in (a). It is seen that unlike $dI/dV(0)$, the sub-gap conductance is showing a fairly universal linear scaling as a function of H/H_{c2} for different T .

As follows from Figs. 2 (g) and (h), state conservation implies that the deficit of the sub-gap conductance is directly connected to the excess of the sum-gap peak, i.e., the deficit of the sum-gap resistance. Fig. 5 (c) shows magnetic field dependence of the sum-gap resistance. It is showing an almost universal, slightly non-linear scaling as a function of H/H_{c2} in the wide T -range.

Fig. 5 (d) shows magnetic field dependence of the sum-gap peak voltage V_p normalized by that at zero field. It exhibits a very simple universal linear scaling as a function of H/H_{c2} in the whole T -range. Interestingly, the peak voltage does not go to zero at $H = H_{c2}$, but rather stops half-way at $eV \simeq \Delta(H = 0)$. This is due to an interplay between the reduction of $\Delta(H)$, see Fig. 1 (b), which moves the peak down, and simultaneous strong smearing of the maximum in the QP DOS, see Fig. 1 (c), which moves the peak up in voltage. At $H = H_{c2}$, Δ does vanish, but voltages/energies of very broad maxima in dI/dV or spatially averaged DOS do not vanish [44], as can be seen from Fig. 4 (b).

C. Extraction of H_{c2} for Nb

The universal scaling of the sum-gap peak voltage $V_p(H/H_{c2})$ can be used for extraction of H_{c2} from magnetotunneling data. Symbols in Fig. 5 (d) show the results of fitting for the Nb/AlAlO_x/Nb junction, using $H_{c2}(T)$ as the only adjustable parameter. It is seen that the agreement with theoretical calculations is excellent. T -dependence of the obtained upper critical field is shown in Fig. 5 (e). Due to the proximity effect in Al it is more linear at low T than that for pure Nb. A similar $H_{c2}^{\perp}(T)$ was also reported for proximity coupled Nb/Cu multilayers [70].

Using thus extracted H_{c2} , we check the scaling of other experimental parameters such as the zero bias and the sub-gap conductances and the sum-gap resistance, shown by symbols in Figs. 5 (a), (b) and (c). In all cases the

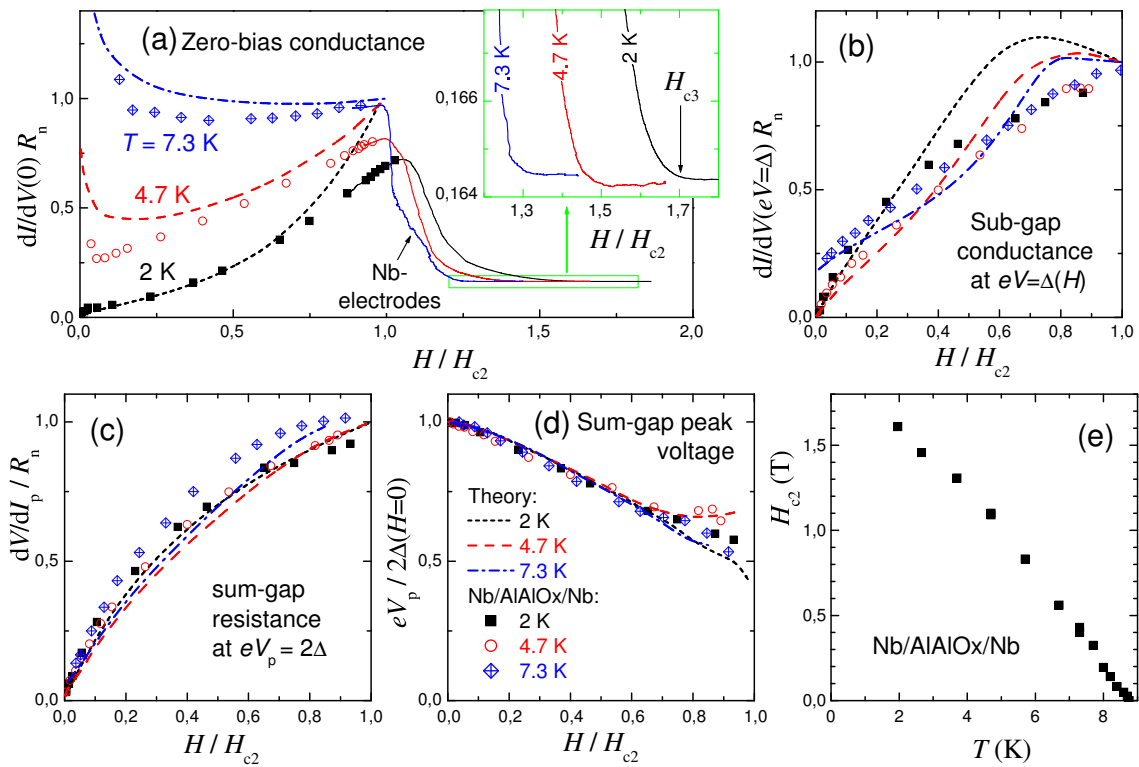


FIG. 5. (Color online). Analysis of scaling of magnetotunneling characteristics at different T as a function of H/H_{c2} in theory (thick lines) and for the Nb junction (symbols). (a) Zero bias conductance. Note that there is no scaling of $dI/dV(0)$ for different T due to progressive development of the zero-bias logarithmic singularity with increasing T . Thin solid lines and the inset show evolution of the conductance of Nb-electrodes at $H > H_{c2}$. It is seen that the surface superconductivity in electrodes survives up to $H_{c3} \simeq 1.69H_{c2}$. (b) Scaling of the sub-gap conductance at finite bias $V = \Delta/e$. (c) Scaling of the sum-gap resistance. (d) Scaling of the sum-gap peak voltage. (e) The upper critical field for Nb, extracted from the scaling.

agreement with theory is very good, confirming the correctness of determination of H_{c2} .

D. Surface superconductivity above H_{c2} in Nb

The only case where there is a certain disagreement between theory and experiment is $dI/dV(0)$ at high fields in Fig. 5 (a): experimental data at $T = 2$ K and 4.7 K is clearly not reaching the normal conductance at $H = H_{c2}$. At higher fields it is not possible to measure junction characteristics because the Nb electrodes are no longer capable to carry the supercurrent and turn into the resistive state. Since the electrode resistance is several times larger than that of the junction, the measured resistance in this case is mostly given by the longitudinal resistances of the Nb electrodes. This leads to the drastic decrease in the measured zero-bias conductance, as shown by thin solid lines in Fig. 5 (a). From this data it is obvious that some residual superconductivity in the Nb electrodes is remaining up to fields significantly larger than H_{c2} .

The inset in Fig. 5 (a) shows the detailed view of the onset of the superconducting transition in Nb electrodes. It is seen that at low $T = 2$ K superconductivity

in Nb survives up to almost exactly $1.69H_{c2}$, which is the expected value of the third critical field H_{c3} . At $H_{c2} < H < H_{c3}$ superconductivity exists only in surface layers. A similar behavior has been reported in clean Nb [71–73] as well as in MgB_2 [74]. From the inset in Fig. 5 (a) it is seen that the ratio H_{c3}/H_{c2} is decreasing with increasing temperature. A similar behavior was reported for clean Nb and discussed in terms of a tricritical point [71]. However, it should be noted that our Nb films are in the dirty limit and are affected by the proximity effect with Al. The columnar structure of sputtered Nb films with a large effective surface-to-volume ratio and columns orientation perpendicular to the film may also enhance the role of surface superconductivity in the out-of-plane magnetic field.

VI. ANALYSIS OF INTRINSIC MAGNETOTUNNELING IN BI-2212

Observation of a fairly conventional behavior of tunneling MR in overdoped Bi(Pb)-2212 encourage us to employ the derived scaling laws for extraction of the T -dependent upper critical field, which remains a contro-

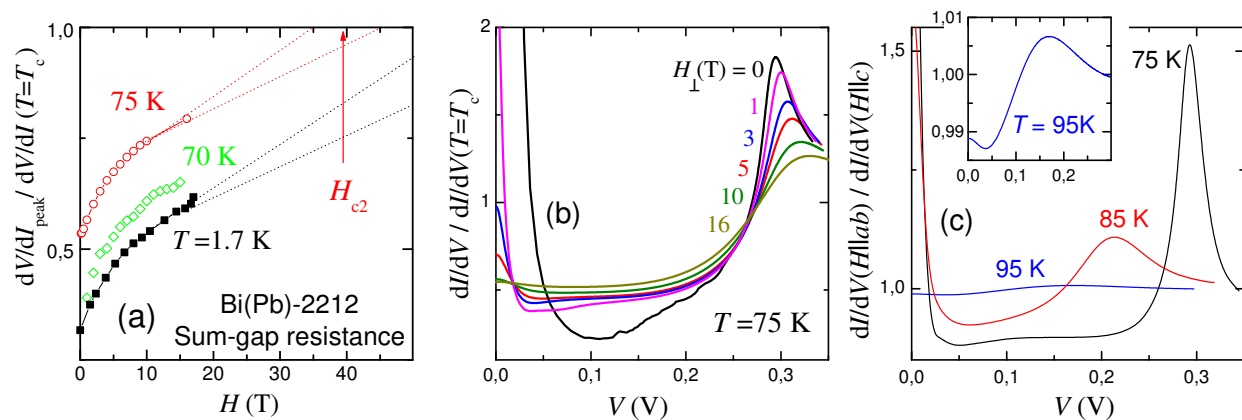


FIG. 6. (Color online). (a) Field-dependence of the sum-gap resistance in Bi(Pb)-2212 at different T (normalized to the normal state value). Dotted lines indicate extrapolations to $H = H_{c2}$. (b) Magnetic field evolution of $dI/dV(V)$ curves at $T = 75$ K (normalized by $dI/dV(V)$ at $T \simeq T_c$). (c) Relative change of dI/dV upon rotation of the crystal in field $H = 10$ T from the in-plane to the c -axis direction. Inset shows enhanced view of the curve at $T = 95$ K.

versial issue for cuprates, as mentioned in the introduction. The obtained scaling of the sum-gap peak voltage $V_p(H/H_{c2})$ is valid not only for tunnel junctions made of s -wave superconductors. A similar scaling was also reported for $\Delta(H/H_{c2})$ in the mixed state of d -wave superconductors [51]. In the remaining part of this work we apply the scaling rules for Bi(Pb)-2212 mesas in order to understand how normal or abnormal the behavior of intrinsic tunneling magnetoresistance is and in an attempt to estimate the upper critical field.

A. Scaling of the sum-gap peak

As seen from Fig. 4 (c), at low T $dI/dV(V)$ characteristics of the Bi(Pb)-2212 mesa, normalized by the normal state dI/dV , behaves in a conventional manner: the sum-gap peak is smeared and moves to lower voltage with increasing the c -axis component of the field. Solid squares in Fig. 6 (a) represent the corresponding peak resistance as a function of field. Apparently, it follows the same tendency of quasi-linear growth as for Nb-junction, shown in Fig. 5 (c). This allows an approximate estimation of H_{c2} by linear extrapolation of the curves to unity, as shown by dotted lines.

Figure 6 (b) shows magnetic field dependence of $dI/dV(V)$ for the mesa from Fig. 3 (d) at $T = 75$ K. Here we also normalized the $dI/dV(V)$ curves by that above T_c . It is seen that the general behavior of the tunneling MR is the same as at low T : the sub-gap conductance increases (negative MR) at the expense of the sum-gap conductance peak (positive MR) in the state-conserving manner. The corresponding peak resistances are shown by open circles in Fig. 6 (a). However, the sum-gap peak is no longer moving to lower voltages with increasing H , but instead spreads out to higher voltages. As discussed

in Ref. [44], such a behavior is not totally unusual. As a matter of fact the upturn of the peak voltage for high H and T is also observed in theory and for Nb/AlAlOx/Nb junctions, even though in a smaller scale, see curves at $T = 4.7$ K in Fig. 5 (d). As discussed above, the outward motion of the peak is the consequence of smearing of the peak in DOS, rather than the actual increase of Δ . This is also the reason why V_p does not go to zero at $H \rightarrow H_{c2}$, despite Δ does vanish.

Figure 6 (c) shows the ratio of conductances at $H = 10$ T oriented parallel to ab -planes (which, as demonstrated in Fig. 3 (d) is equivalent to zero-field) and in the c -axis direction. Such a normalization perfectly removes all field independent features and allows observation with unprecedented clarity superconducting parts of the spectra at $T \rightarrow T_c$. In Fig. 6 (c) we clearly see the sum-gap peak at $T = 85$ K, which is practically indistinguishable in $dI/dV(V)$ characteristics. Remarkably, we can observe the peak even at $T = 95$ K (see the inset), which is above the critical temperature for appearance of phase-coherence in the c -axis direction $T_c^{phase} = 91 - 92$ K. Apparently the superconducting gap is still present at 95 K, but its value is rapidly decreasing at this temperature, as it does in BCS theory close to the mean-field T_{c0} , see Fig. 2 (f). This is consistent with the conclusion of Ref. [13] that superconductivity in near optimally doped Bi-2212 appears by means of the second-order phase transition in the conventional BCS-manner. However, the true thermodynamic mean-field critical temperature $T_{c0} \simeq 96$ K is somewhat higher than T_c^{phase} .

B. Scaling of the sub-gap voltage

As seen from Fig. 3 (c), the voltage at a given current is decreasing with increasing field and reaches the normal

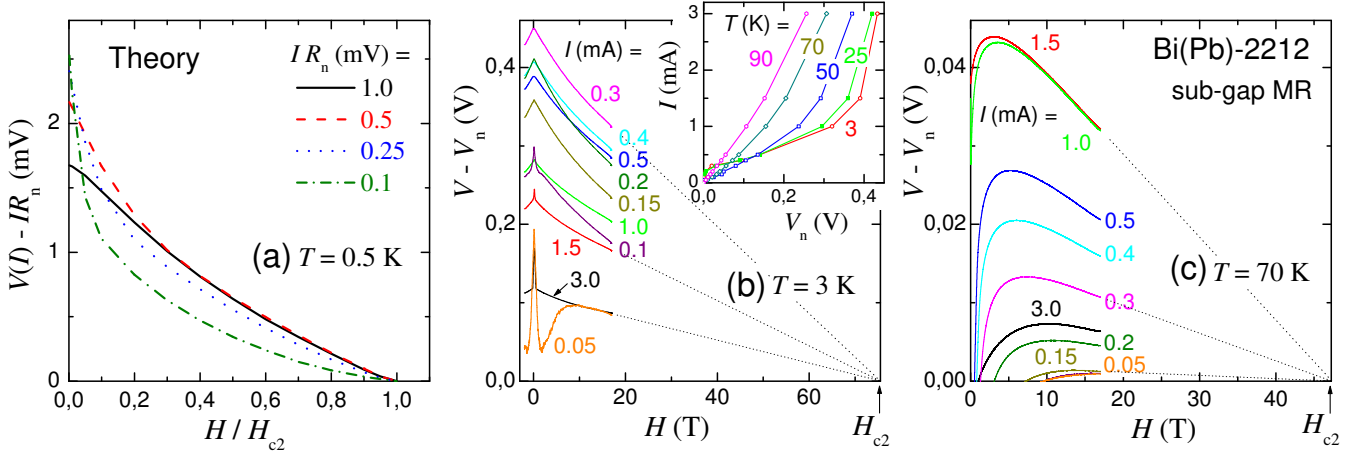


FIG. 7. (Color online). Magnetic field dependence of the voltage at a given current for (a) theoretical calculation, current levels correspond to horizontal lines in Fig. 3 (c), and for Bi(Pb)-2212 mesa at (b) $T = 3$ K and (c) $T = 70$ K at different bias currents. Inset in (b) shows normal-state $I - V$ s obtained by adjustment of $V - V_n$ so that they vanish at the same $H = H_{c2}$, as indicated by dotted lines in (b) and (c).

state value $V_n(I) = IR_n$ at $H = H_{c2}$. Fig. 7 (a) shows the corresponding values of $V(I, H)$ for four bias currents, indicated by horizontal lines in Fig. 3 (c), as a function of H/H_{c2} . It is seen that in a wide bias range (an order of magnitude) $V(I, H) - IR_n$ have the same magnitude and disappears in a linear manner at $H \rightarrow H_{c2}$. This fairly good and almost bias-independent scaling is the consequence of the almost parallel shift of $I - V$ s (in the semi-logarithmic scale) with increasing H , as shown in Figs. 3 (c), . The $dI/dV(V)$ curves behave in the same manner, as shown in Fig. 4.

Fig. 3 (d) demonstrates that for Bi(Pb)-2212 such parallel translation of $I - V$ curves is even more impressive and expands to almost two orders of magnitude in bias current. However, there is one major obstacle for determination of the H_{c2} from such the scaling. Namely, the shape of the $I - V$ in the normal state, i.e., with completely suppressed superconductivity but at low $T < T_c$, is unknown. We can only say for sure that it remains non-linear above T_c as a result of thermal-activation c -axis transport (not necessarily connected with the pseudogap) [34]. To go around this problem, we note that according to Fig. 7 (a), voltages at all bias levels must reach the normal state values $V_n(I)$ in a quasi-linear manner at the same $H = H_{c2}$. Therefore, we used $V_n(I)$ as an adjustable parameter for each bias current, so that all $V(I) - V_n(I)$ voltages go to zero at the same point $H = H_{c2}(T)$, as indicated by dotted lines in Figs. 7 (b) and (c). Thus obtained normal state $I - V$ curves at $T < T_c$ are shown in the inset of Fig. 7 (b).

Figure 7 (b) and (c) show H_{\perp} -dependence of the sub-gap voltages at different bias currents, for (b) $T = 3$ K and (c) 70 K. We observe a quasi-linear reduction of voltages, consistent with theoretical curves in Fig. 7 (a). The extrapolated value of H_{c2} at $T = 3$ K is 75.5 ± 14.5 T. A significant uncertainty is due to the need for

remote extrapolation from the maximum available field of 17 T. However, at low T it is not crucially affected by the adjustment of V_n . Indeed, already from the raw data in Fig. 3 (d) it is seen that in fields from 0 to 17 T the $I - V$ curves made approximately 1/4–1/5 of the journey to the normal state $I - V$ at $T = 90$ K. Assuming a linear dependence of $V(H)$, this provides a similar estimation of $H_{c2} \sim 68 - 85$ T.

C. Temperature dependence of the maximum c -axis magnetoresistance

Fig. 8 (a) shows temperature dependence of the maximum measured shift of voltage at a constant current upon variation of the c -axis magnetic field from 0 to 17 T. It is seen that the negative sub-gap tunneling MR is rapidly decreasing with increasing temperature, cf. scales in Figs. 7 (b) and (c). This makes determination of H_{c2} at elevated T less confident because it becomes more sensitive to exact values of V_n . For comparison, Fig. 8 (b) shows similar data for the Nb-junction at $H = 0.44$ T, which corresponds to the same ratio $H/H_{c2}(T = 0) \simeq 0.24$ as for Bi(Pb)-2212 from panel (a). The tunneling MR in the Nb-junction vanishes at $T \simeq 7$ K $< T_c$, at which $H_{c2}(T) = H$, see Fig. 5 (e).

From comparison of Figs. 8 (a) and (b) it is seen that behavior of the maximum MR is qualitatively similar for Nb and Bi(Pb)-2212. However, for Bi(Pb)-2212 it becomes more smeared and fuzzy at $T \rightarrow T_c$. To some extent the smoother T -dependence for Bi-2212 may be caused by the d -wave symmetry, because nodal QP's are more prone to thermal activation above the gap at elevated T . Still this does not explain everything.

The inset in Fig. 8 (a) shows the same data for Bi(Pb)-2212 in the semi-logarithmic scale. It is seen that the sub-

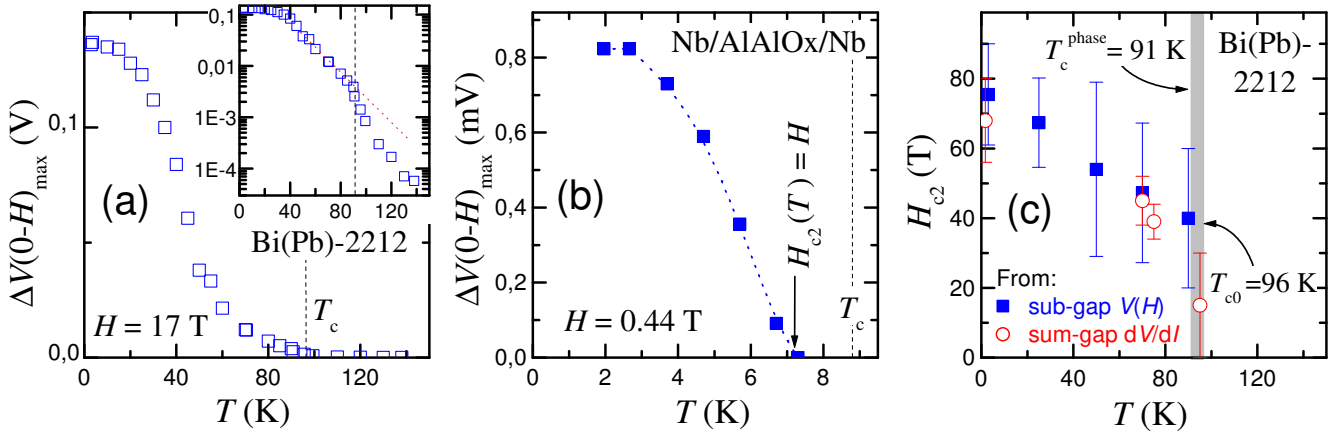


FIG. 8. (Color online). Temperature dependence of the maximum magnetoresistance at a constant current, $\Delta V(0 - H) = V(I, H = 0) - V(I, H)$, (a) for Bi(Pb)-2212 mesas at $H = 17$ T, (b) for the Nb/AlAlOx/Nb junction at $H \simeq 0.44$ T with the same $H/H_{c2}(0)$ ratio. The inset in (a) shows the same data in the semi-logarithmic scale. It is seen that the negative sub-gap magnetoresistance decays almost exponentially with increasing T , but retains a finite value at $T > T_c$. (c) Extracted upper critical field in the c -axis direction for Bi(Pb)-2212.

gap MR start to rapidly decrease (approximately exponentially) with increasing temperature at $40 \text{ K} < T < T_c$ (as indicated by the dotted line), experiences an additional drop at T_c (marked by the dashed vertical line) and then continued to decrease at even faster rate above T_c . We assume that the remaining small negative MR above T_c is a consequence of fluctuation superconductivity, which becomes progressively less sensitive to magnetic field due to growth of the effective $H_{c2}^* \propto T - T_c$ above T_c [29].

D. Extraction of H_{c2} for Bi-2212

As follows from Fig. 5 (c), scaling of sum-gap magnetoresistance provides the most accurate way of determination of H_{c2} . The corresponding data for Bi(Pb)-2212 are shown in Fig. 6 (a). Data for 1.7 K and 75 K correspond to Figs. 4 (d) and 6 (b). The upper critical field is estimated using a linear extrapolation towards the normal resistance, as indicated by dotted lines. There is a significant uncertainty in such extrapolation, however it is more robust than that made from sub-gap MR, see Fig. 7, because the normal resistance at a large bias is more unambiguous and has a weak T -dependence [7, 34], as seen from Fig. 2 (c).

Figure 8 (c) shows the extracted T -dependence of the upper critical field for the slightly overdoped Bi(Pb)-2212 single crystal. Solid squares and open symbols are obtained from analysis of scaling of the sub-gap voltage, Figs. 7 (b) and (c), and the sum-gap resistance, Fig. 6 (a), respectively. $H_{c2}(T = 0)$ is ~ 70 T and certainly decreases with increasing T . As mentioned in the introduction, one of the principle questions is whether H_{c2} goes to zero at T_c . This appears to be a difficult question. First, the notion of T_c is fuzzy, as indicated by the

gray area in Fig. 8. We see the clear presence of the superconducting gap in the DOS above the phase coherent $T_c^{\text{phase}} \simeq 91$ K up to the mean-field $T_{c0} \simeq 96$ K [13]. The main experimental challenge is associated with a very small sub-gap MR close to T_c , see Fig. 8 (a). However, at $T = 95$ K any sign of the sum-gap peak is absent at $H = 15$ T, which provides a rough estimation for the last point in the $H_{c2}(T)$ diagram of Fig. 8 (c).

VII. CONCLUSIONS

We performed a detailed comparative analysis of tunneling magnetoresistances in conventional low- T_c Nb/AlAlOx/Nb junctions, small Bi(Pb)-2212 intrinsic Josephson junctions and microscopic calculations. It was found that magnetotunneling in slightly overdoped Bi(Pb)-2212 is qualitatively similar to that in conventional BCS-type superconductors.

From the data presented above it is clearly seen that both temperature and magnetic field suppress superconductivity in Bi(Pb)-2212 in the state conserving manner. Magnetotunneling provides a particularly clear demonstration of this: due to conservation of states the MR changes sign from the negative in the sub-gap, to the positive at the sum-gap bias. Continuing strong MR well above the sum-gap peak with powers up to several times that on the peak indicate that the mesa remains in the superconducting state and the peak is not caused by self-heating. This clearly demonstrates that intrinsic tunneling can provide unambiguous information about bulk electronic spectra of Bi-2212.

Observation of state conservation implies that QP states released upon suppression of superconductivity by magnetic field are not taken over by a competing order, like charge or spin density wave. In other words, there

is no field-induced non-superconducting order in slightly overdoped Bi(Pb)-2212. The situation may, however be different for underdoped Bi-2212, for which non-state-conserving characteristics have been reported [36, 75].

We derived theoretically and verified experimentally scaling laws of various magnetotunneling parameters. Those scaling laws were employed for accurate extraction of the upper critical fields and in the case of Nb provided a clear evidence for the existence of an extended region of surface superconductivity at $H_{c2} < H < H_{c3}$.

For Bi(Pb)-2212, it was found that $H_{c2}(T = 0) \simeq 70$ T and decreases significantly upon approaching T_c . The parameters of Bi(Pb)-2212 were obtained from self-consistent analysis of magnetotunneling data at different levels of bias, dissipation powers and different mesa sizes, which precludes the influence of self-heating. The amplitude of the sub-gap magnetoresistance is suppressed ex-

ponentially at $T > T_c/2$. It remains negative, although very small, above T_c , probably indicating existence of an extended fluctuation region.

We conclude in general that intrinsic magnetotunneling in small mesa structures is a very powerful tool for analysis of bulk superconducting properties of cuprates.

ACKNOWLEDGMENTS

We are grateful to A. Golubov for assistance with numerical simulations, D. Haviland for providing Nb/AlAlOx/Nb junctions, and to A. Kordyuk, S. Borisenko, D. Munzar and Ch. Bernhard for stimulating discussions. Financial support from the Swedish Research Council, the SU-Core Facility in Nanotechnology and the K.&A. Wallenberg foundation is gratefully acknowledged.

-
- [1] D. LeBoeuf, N. Doiron-Leyraud, B. Vignolle, M. Sutherland, B.J. Ramshaw, J. Levallois, R. Daou, F. Laliberte, O. Cyr-Choiniere, J. Chang, Y.J. Jo, L. Balicas, R. Liang, D.A. Bonn, W.N. Hardy, C. Proust, and L. Taillefer *Phys. Rev. B* **83**, 054506 (2011).
- [2] T. Helm, M.V. Kartsovnik, M. Bartkowiak, N. Bittner, M. Lambacher, A. Erb, J. Wosnitzer and R. Gross *Phys. Rev. Lett.* **103**, 157002 (2009).
- [3] S. Hüfner, M.A. Hossain, A. Damascelli, and G.A. Sawatzky, *Rep. Prog. Phys.* **71**, 062501 (2008).
- [4] D.N. Basov and T. Timusk, *Rev. Mod. Phys.* **77**, 721 (2005).
- [5] M.R. Norman, D. Pines, and C. Kallin, *Adv. Phys.* **54**, 715 (2005).
- [6] Ø. Fisher, M. Kugler, I. Maggio-Aprile, Ch. Berthod, and Ch. Renner, *Rev. Mod. Phys.* **79**, 353 (2007).
- [7] V.M. Krasnov, A. Yurgens, D. Winkler, P. Delsing and T. Claeson, *Phys. Rev. Lett.* **84**, 5860 (2000).
- [8] J. Demsar, B. Podobnik, V.V. Kabanov, Th. Wolf, and D. Mihailovic, *Phys. Rev. Lett.* **82**, 4918 (1999).
- [9] L. Yu, D. Munzar, A.V. Boris, P. Yordanov, J. Chaloupka, Th Wolf, C.T. Lin, B. Keimer and Ch. Bernhard, *Phys. Rev. Lett.* **100**, 177004 (2008).
- [10] Y. Yamada, K. Anagawa, T. Shibauchi, T. Fujii, T. Watanabe, A. Matsuda and M. Suzuki, *Phys. Rev. B* **68**, 054533 (2003).
- [11] W.S. Lee, I.M. Vishik, K. Tanaka, D.H. Lu, T. Sasagawa, N. Nagaosa, T.P. Devereaux, Z. Hussain and Z.X. Shen, *Science* **450**, 81 (2007).
- [12] M. LeTacon, A. Sacuto, A. Georges, G. Kotliar, Y. Galais, D. Colson, and A. Forget, *Nature Phys.* **2**, 537 (2006)
- [13] V.M. Krasnov, *Phys. Rev. B* **79**, 214510 (2009).
- [14] V.M. Krasnov, *Phys. Rev. B* **65**, 140504(R) (2002).
- [15] J.L. Tallon and J.W. Loram, *Physica C* **349**, 53 (2001).
- [16] V.M. Krasnov, A.E. Kovalev, A. Yurgens, and D. Winkler, *Phys. Rev. Lett.* **86**, 2657 (2001).
- [17] A.D. LaForge, W.J. Padilla, K.S. Burch, Z.Q. Li, A.A. Schafgans, K. Segawa, Y. Ando and D.N. Basov, *Phys. Rev. Lett.* **101**, 097008 (2008).
- [18] M.H. Bae, J.H. Choi, H.J. Lee, and K.S. Park, *J. Kor. Phys. Soc.* **48**, 1017 (2006).
- [19] H.K. Nguyen and S. Chakravarty, *Phys. Rev. B* **65**, 180519(R) (2002).
- [20] A. Kanigel, U. Chatterjee, M. Randeria, M.R. Norman, G. Koren, K. Kadowaki, and J.C. Campuzano, *Phys. Rev. Lett.* **101**, 137002 (2008).
- [21] Y. Wang, L. Li, and N.P. Ong, *Phys. Rev. B* **73**, 024510 (2006).
- [22] F. Bouquet, L. Fruchter, I. Sfar, Z.Z. Li, and H. Raffy, *Phys. Rev. B* **74**, 064513 (2006).
- [23] G.C. Kim, M. Cheon, H. Kim, Y.C. Kim, and D.Y. Jeong, *Phys. Rev. B* **72**, 064525 (2005).
- [24] Y. Ando, G.S. Boebinger, A. Passner, L.F. Schneemeyer, T. Kimura, M. Okuya, S. Watauchi, J. Shimoyama, K. Kishio, K. Tamasaku, N. Ichikawa, and S. Uchida, *Phys. Rev. B* **60**, 12475 (1999).
- [25] B. Rosenstein, B.Y. Shapiro, R. Prozorov, A. Shaulov and Y. Yeshurun, *Phys. Rev. B* **63**, 134501 (2001)
- [26] B.J. Taylor, R.E. Baumbach, D.J. Scanderbeg, and M.B. Maple, *Phys. Rev. B* **81**, 174511 (2010).
- [27] L. Krusin-Elbaum, G. Blatter, and T. Shibauchi, *Phys. Rev. B* **69**, 220506 (2004).
- [28] A.A. Kordyuk, S.V. Borisenko, A. Koitzsch, J. Fink, M. Knupfer, B. Büchner and H. Berger, *J. Phys. Chem. Sol.* **67**, 201 (2006).
- [29] A.I. Larkin and A.A. Varlamov, Fluctuation Phenomena in Superconductors, arXiv:cond-mat/0109177
- [30] V.F. Mitrovic, E.E. Sigmund, W.P. Halperin, A.P. Reyes, P. Kuhns, and W.G. Moulton, *Phys. Rev. B* **67**, 220503(R) (2003).
- [31] R. Kleiner and P. Müller, *Phys. Rev. B* **49**, 1327 (1994).
- [32] P.A. Warburton, S. Saleem, J.C. Fenton, M. Korsah, and C.R.M. Grovenor, *Phys. Rev. Lett.* **103**, 217002 (2009).
- [33] S. Ueda, T. Yamaguchi, Y. Kubo, S. Tsuda, Y. Takano, J. Shimoyama and K. Kishio, *J. Appl. Phys.* **106**, 074516 (2009).
- [34] S.O. Katterwe, A. Rydh and V.M. Krasnov, *Phys. Rev. Lett.* **101**, 087003 (2008).
- [35] A. Yurgens, D. Winkler, T. Claeson, G. Yang, I.F.G. Parker, and C.E. Gough, *Phys. Rev. B* **59**, 7196 (1999).

- [36] K. Anagawa, Y. Yamada, T. Watanabe and M. Suzuki, *Phys. Rev. B* **67**, 214513 (2003).
- [37] S.I. Vedeneev, B.A. Piot, and D.K. Maude, *Phys. Rev. B* **81**, 054501 (2010).
- [38] E. Guyon, A. Martinet, J. Marticon, and P. Pincus, *Phys. Rev.* **138**, A746 (1965).
- [39] R.S. Colliner and R.A. Kamper, *Phys. Rev.* **143**, 323 (1966).
- [40] J. Millstein and M. Tinkham, *Phys. Rev.* **158**, 325 (1967).
- [41] P.Szabo, P. Samuely, A.G. M. Jansen, J. Marcus and P. Wyder, *Phys. Rev. B* **62**, 3502 (2000).
- [42] I. Vekhter, L.N. Bulaevskii, A.E. Koshelev, and M.P. Maley, *Phys. Rev. Lett.* **84**, 1296 (2000).
- [43] N. Morozov, L. Krusin-Elbaum, T. Shibauchi, L.N. Bulaevskii, M.P. Maley, Yu.I. Latyshev and T. Yamashita, *Phys. Rev. Lett.* **84**, 1784 (2000).
- [44] V.M. Krasnov, *Physica C* **408-410**, 405 (2004).
- [45] V.M. Krasnov, A. Yurgens, D. Winkler and P. Delsing, *J. Appl. Phys.* **89**, 5578 (2001).
- [46] V.M. Krasnov, M. Sandberg, and I. Zogaj, *Phys. Rev. Lett.* **94**, 077003 (2005).
- [47] R. Watts-Tobin, L. Kramer, and W. Pesch, *J. Low Temp. Phys.* **17**, 71 (1974).
- [48] A.A. Golubov and M.Yu. Kupriyanov, *J. Low Temp. Phys.* **70**, 83 (1988).
- [49] A.A. Golubov and U. Hartmann, *Phys. Rev. Lett.* **72**, 3602 (1994).
- [50] A.A. Golubov, E.P. Houwman, J.G. Gijsbertsen, V.M. Krasnov, J. Flokstra, H. Rogalla, and M.Yu. Kupriyanov, *Phys. Rev. B* **51**, 1073 (1995).
- [51] M. Ichioka, A. Hasegawa, and K. Machida, *Phys. Rev. B* **59**, 8902 (1999).
- [52] N.B. Kopnin and G.E. Volovik, *JETP Lett.* **64**, 690 (1996).
- [53] N.E. Hussey, *Adv. Phys.* **51**, 1685 (2002).
- [54] M.M. Maska and M. Mierzejewski, *Phys. Rev. B* **68**, 024513 (2003).
- [55] J.X. Zhu, and C.S. Ting, *Phys. Rev. Lett.* **87**, 147002 (2001).
- [56] J.F. Zasadzinski, L. Ozyuzer, N. Miyakawa, K.E. Gray, D.G. Hinks, and C. Kendziora, *Phys. Rev. Lett.* **87**, 067005 (2001).
- [57] S. O. Katterwe, A. Rydh, H. Motzkau, A. B. Kulakov, V. M. Krasnov, *Phys. Rev. B* **82**, 024517 (2010).
- [58] HYPRES, Inc., Elmsford, NY 10523 USA.
- [59] S.K. Tolpygo, D. Yohannes, R.T. Hunt, J.A. Vivalda, D. Donnelly, D. Amparo, and A.F. Kirichenko, *IEEE Trans. Appl. Supercond.* **17**, 946 (2007).
- [60] V.M. Krasnov, *ArXiv: 1007.4510*.
- [61] A.B. Kulakov, I.K. Bdikin, S.A. Zver'kov, G.A. Emel'chenko, G. Yang, J.S. Abell, *Physica C* **371**, 45 (2002).
- [62] V.M. Krasnov, T. Bauch, and P. Delsing, *Phys. Rev. B* **72**, 012512 (2005).
- [63] V.M. Krasnov, *Phys. Rev. Lett.* **97**, 257003 (2006).
- [64] V.M. Krasnov, T. Golod, T. Bauch, and P. Delsing, *Phys. Rev. B* **76**, 224517 (2007).
- [65] A. Dubrovka, L. Yu, D. Munzar, K.W. Kim, M. Rössle, V.K. Malik, C.T. Lin, B. Keimer, Th Wolf, and Ch. Bernhard, *Eur. Phys. J.* **188**, 73 (2010).
- [66] V.M. Krasnov, *Physica C* **372-376**, 103 (2002).
- [67] S.O. Katterwe, H. Motzkau, A. Rydh, and V.M. Krasnov, *Phys. Rev. B* **83**, 100510(R) (2011).
- [68] M. Giura, R. Fastampa, S. Sarti, and E. Silva, *Phys. Rev. B* **68**, 134505 (2003).
- [69] A.I. Larkin and Yu.N. Ovchinnikov, *Sov. Phys. JETP* **24**, 1035 (1967).
- [70] V.M. Krasnov, A.E. Kovalev, V.A. Oboznov, and N.F. Pedersen, *Phys. Rev. B* **54**, 15448 (1996).
- [71] S.R. Park, S.M. Choi, D.C. Dender, J.W. Lynn, and X.S. Ling, *Phys. Rev. Lett.* **91**, 167003 (2003).
- [72] J. Kötzler, L. von Sawilski, and S. Casalbuoni, *Phys. Rev. Lett.* **92**, 067005 (2004).
- [73] P. Das, C.V. Tomy, S.S. Banerjee, H. Takeya, S. Ramakrishnan, and A.K. Grover, *Phys. Rev. B* **78**, 214504 (2008).
- [74] A. Rydh, U. Welp, J.M. Hiller, A.E. Koshelev, W.K. Kwok, G.W. Crabtree, K.H.P. Kim, K.H. Kim, C.U. Jung, H.-S. Lee, B. Kang, and S.-I. Lee, *Phys. Rev. B* **68**, 172502 (2003).
- [75] A.K. Gupta and K.-W. Ng, *Europhys. Lett.* **58**, 878 (2002).